Atomic Structure of ABC Rhombohedral Stacked Trilayer Graphene

Jamie H. Warner,[†,*] Masaki Mukai,[‡] and Angus I. Kirkland[†]

[†]Department of Materials, University of Oxford, Parks Road, Oxford, OX1 3PH, United Kingdom and [‡]JEOL Ltd, 3-1-2 Musashino, Akishima, Tokyo 196-8558, Japan

ABSTRACT

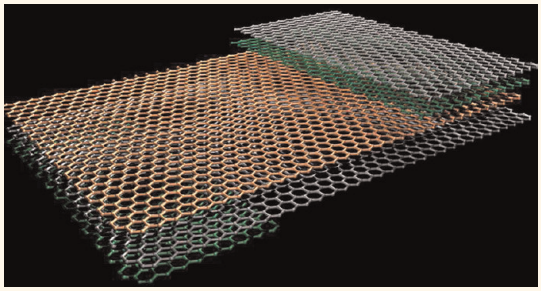

We distinguish between Bernal and rhombohedral stacked trilayer graphene using aberration-corrected high-resolution transmission electron microscopy. By using a monochromator to reduce chromatic aberration effects, angstrom resolution can be achieved at an accelerating voltage of 80 kV, which enables the atomic structure of ABC rhombohedral trilayer graphene to be unambiguously resolved. Our images of ABC rhombohedral trilayer graphene provide a clear signature for its identification. Few-layer graphene interfaces with ABC:BC:BCAB structure have also been studied, and we have determined the stacking sequence of each graphene layer and consequently the 3D structure. These results confirm that CVD-grown few-layer graphene can adopt an ABC rhombohedral stacking.

KEYWORDS: trilayer graphene · ABC · rhombohedral · CVD · HRTEM

Monolayer, bilayer, and trilayer graphene have fundamentally different electronic properties, and the relative orientation between each layer of graphene in these 1−3 sheet systems influences their behavior.[1−7] Few-layer graphene is known to generally adopt AB Bernal stacking, but more recently evidence of rhombohedral stacking has also emerged.[8,9] For trilayer graphene a mixture of both ABC rhombohedral stacking and ABA Bernal stacking has been predicted. Recent experimental studies have revealed that ABC trilayer graphene, as identified by a peak asymmetry in Raman spectroscopy,[8] has different electrical properties compared to ABA Bernal trilayer graphene.[6]

A fully resolved atomic structure is an important component in accurate structure−property relationships, which underpin the development of future applications. In this regard, scanning tunnelling microscopy (STM) and transmission electron microscopy (TEM) have emerged as the optimal methods for obtaining atomically resolved structural information. STM is optimized for studies of graphene residing on surfaces, while TEM is best suited to studies of freely suspended graphene, which do not suffer from complications due to substrate interactions.

Atomic resolution imaging of graphene has been dramatically enhanced by the development of spherical aberration correctors, and it is now routinely possible to observe lattice structure of graphene using commercial TEM systems operating at 80 kV.[10−12] Scanning transmission electron microscopy is also capable of resolving lattice structure in graphene.[13] However, in order to fully resolve the structure of graphene in mono-, bi-, and trilayer forms using HRTEM, it is necessary to overcome the resolution limitations imposed by the effects of chromatic aberrations. One solution to this is to reduce the energy spread of the electron beam using a monochromator.[10]

Here, we show how the improved spatial resolution obtained from monochromation of the electron beam using a double Wien filter monochromator, combined with spherical aberration correction, enables a detailed study of the relative stacking orientation between multiple graphene layered structures.

RESULTS/DISCUSSION

Graphene was grown using chemical vapor deposition with a copper metal catalyst using a previously reported method and transferred onto SiN TEM grids with 2 μm holes.[14] Figure 1 shows atomic models for Bernal and rhombohedral stacked trilayer graphene. If a fourth layer is added to a Bernal stacking sequence, it adopts the same position as layer B, and in a rhombohedral stacking sequence the fourth layer matches layer A. HRTEM image simulations

* Address correspondence to Jamie.warner@materials.ox.ac.uk.

Received for review April 24, 2012 and accepted May 22, 2012.

Published online June 04, 2012
10.1021/nn3017926

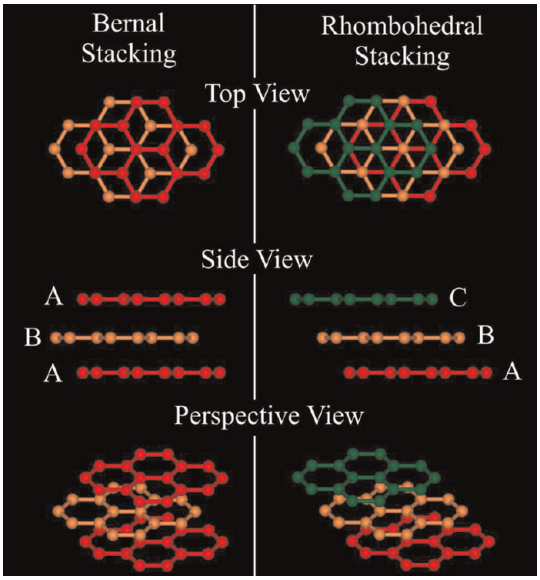

Figure 1. Atomic models of Bernal (ABA) and rhombohedral (ABC) stacked trilayer graphene showing top, side, and perspective views.

using the multislice algorithm performed for a range of defocus values for both ABA and ABC stacked trilayer graphene reveal that ABC stacked trilayer graphene has a unique contrast pattern.[15]

Both ABA and ABC stacking contain a similar bilayer of AB stacked graphene, and we first focus our attention on this and its interface with a monolayer. Figure 2(i, a) and (i, b) show typical HRTEM images obtained without the use of a monochromator for (i, a) monolayer graphene and (i, b) a monolayer–bilayer graphene interface. These images are of similar standard to those previously reported in the literature, in terms of ability to resolve individual carbon atoms and show contrast reversal at the monolayer–bilayer step edge.[10–12,14,16–22] As previously reported, the HRTEM image from bilayer graphene shows similar contrast to monolayer graphene with an overall hexagonal symmetry.[10,23]

Figure 2(ii, a) and (ii, b) show typical HRTEM images obtained using monochromatic illumination (5 μm slit) for (ii, a) a monolayer–bilayer graphene interface recorded with a 2 s acquisition and (ii, b) an averaged image from 17 sequential images to improve signal-to-noise. Contrast from carbon atoms in graphene can be either white or black in HRTEM images, depending on the defocus used to acquire the image. The increased resolution leads to fully resolved carbon atoms within the monolayer graphene, but most interesting is the significant change in contrast for the monolayer–bilayer interface. In order to understand this, we have performed multislice image simulations using the atomic model shown in Figure 2(ii, c) with the resultant simulation shown in Figure 2(ii, d). The simulation was calculated using conditions representative of the microscope with monochromatic illumination as described. A comparison of this atomic model with the image simulation shows that the complex pattern in the bilayer region results from full resolution of the AB Bernal stacking. Where two atoms overlap in projection, strong contrast results, which is surrounded by six weaker contrast spots associated with single carbon atoms in projection. This confirms that our data fully resolve all the atoms in AB Bernal stacking for the first time by direct imaging using HRTEM. Further confirmation is obtained by examining atoms at the edge of graphene, Figure 2(e). Boxed line profiles were taken across two arm-chair directions, Figure 2(f, g), and a double Gaussian fit, shown in red in Figure 2(g), gives peak widths of 76 and 73 pm, indicating resolution near 80 pm.

We now extend this discussion to trilayer graphene, which can adopt both ABA and ABC stacking configurations. Figure 3(i) shows HRTEM image simulations for both ABC and ABA stacked trilayer graphene for different defocus values, using parameters appropriate to the microscope conditions with monochromatic illumination. This demonstrates that ABC trilayer graphene shows a simple inversion of the contrast (black/white) and that all the atomic positions in the image have the same intensity. This ability to distinguish the lattice structure of ABC trilayer graphene, compared to AB and 4 layers of rhombohedral stacked graphene, is examined more closely in Figure 3(ii). An atomic model with a 3:2:4 ABC:BC:BCAB sequence of graphene layers, all rhombohedrally stacked, was used for a series of multislice image simulations in Figure 3(ii), with the resolution variously limited by increasing the defocus spread from (a) 2 nm to (f) 7 nm. Figure 3(ii, g) shows a side view of the layer stackings for the three different regions (1, 2, and 3) as labeled in Figure 3(ii, a). We note that the BC 2-layer rhombohedral stacking is the same as AB Bernal stacking. The simulations in Figure 3(ii, d)–(ii, f) show low contrast in the ABC graphene region, but both the BC and ABCB stacking sequences are resolved for these focal spreads as hexagonal patterns. It is only when the focal spread is less than 4 nm, Figure 3(ii, c), that the simulated image directly corresponds to the ABC graphene structure, and when the focal spread is reduced further, Figure 3(ii, a) and (ii, b), the contrast pattern from the BC graphene region becomes fully representative of the atomic positions. This demonstrates that high spatial resolution is required to unambiguously distinguish ABC graphene from other few-layer graphene structures.

Having established that the key marker for ABC trilayer graphene is its defocus-dependent contrast pattern,[15] we have explored areas of our few-layer graphene sample for this effect. Such a region exhibiting the predicted contrast behavior with variations in defocus is shown in Figure 4(i, a) and (i, b) for two slightly different defocus values. In this region the contrast pattern simply inverts, as expected for ABC rhombohedral stacked trilayer graphene. We have also studied the interface of this ABC trilayer graphene region with other layer numbers to determine the exact layer assignment.

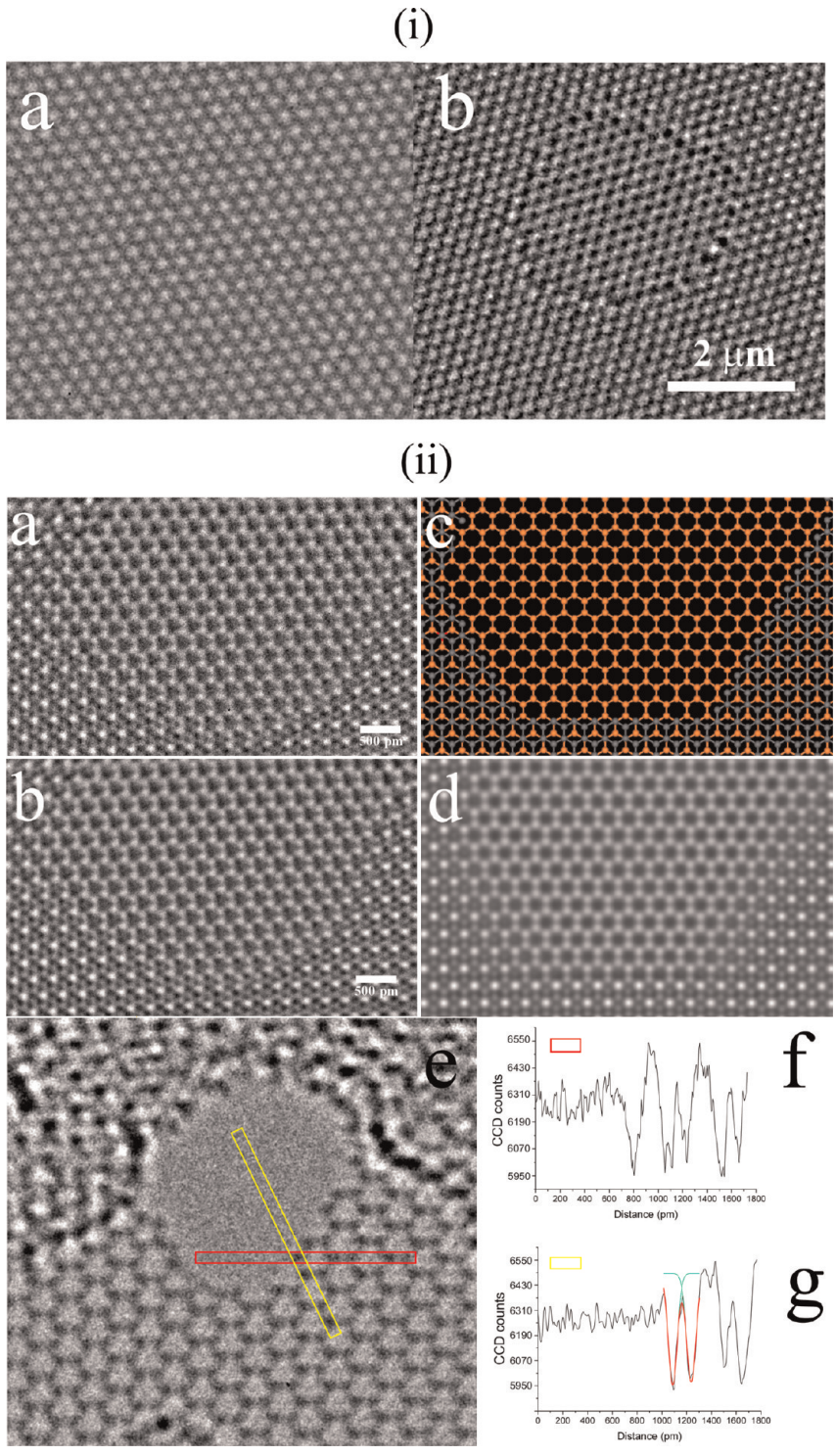

Figure 2. (i) HRTEM image (non-monochromated illumination) of (a) monolayer graphene; (b) monolayer–bilayer interface (monolayer: white atom contrast; bilayer: black atom contrast). (ii) HRTEM images (monochromated illumination) of (a) monolayer–bilayer graphene interface (single 2 s acquisition); (b) same area as in (a) but with 17 sequential frames averaged to improve signal-to-noise; (c) atomic model of a monolayer (orange)–bilayer (gray) interface with AB Bernal stacking; (d) HRTEM image simulation based on the atomic model in (c); (e) HRTEM image of C atoms at the edge of graphene; red (f) and yellow (g) boxes indicate line profile regions. A double Gaussian fit is shown in red in (g) with peak widths of 76 and 73 pm.

Figure 4(ii, a) and (ii, b) show an atomic model of an ABC:BCAB (3:4) rhombodehdral stacked graphene layer interface, and Figure 4(ii, c) and (ii, d) show two HRTEM images taken of such an interface with different defoci. Corresponding image simulations for two defoci are presented below each HRTEM image in Figure 4(ii, e) and (ii, f). This area was then irradiated using a focused electron beam to sputter a hole in the back monolayer of

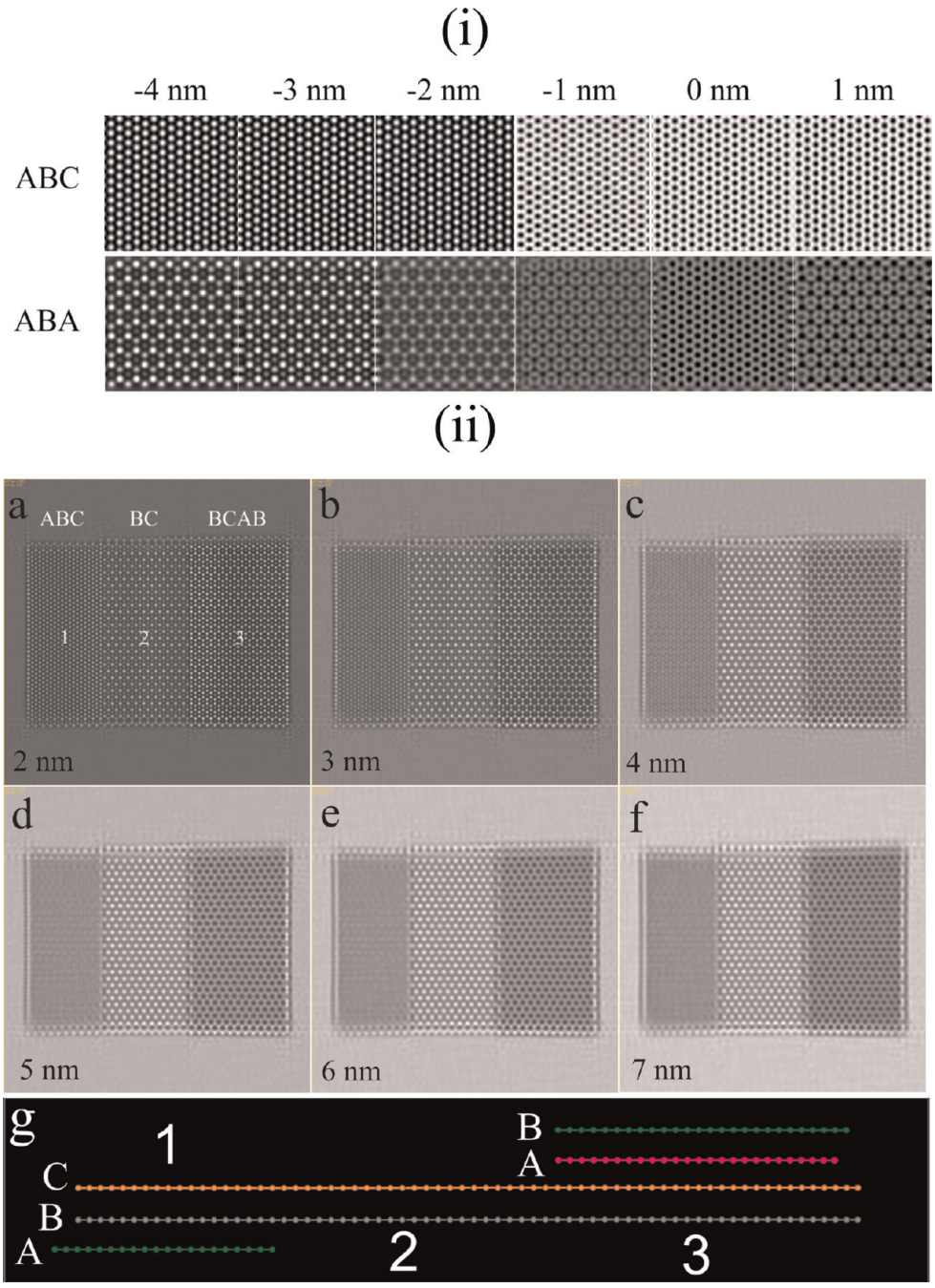

Figure 3. (i) HRTEM image simulations of ABC and ABA trilayer graphene for the different defocus values indicated with other imaging parameters appropriate to the monochromator. (ii) HRTEM image simulations of a 3:2:4 ABC:BC:BCAB graphene layer structure with different defocus spread values of (a) 2 nm, (b) 3 nm, (c) 4 nm, (d) 5 nm, (e) 6 nm, and (f) 7 nm. In (ii, a) region 1 = ABC, region 2 = BC, and region 3 = BCAB.

graphene in order to further explore the layer ordering.[16] This resulted in a hole appearing in a region of the ABC layer, exposing the middle BC layer.

Figure 4(iii, a) shows an atomic model of a 3:2:4 ABC:BC:BCAB graphene layer structure and (b) the side view illustrating the hole sputtered in the bottom A layer (green arrow). Figure 4(ii, c) shows the experimental HRTEM image of the same area as in Figure 4(ii), but with a small hole in the middle following electron beam irradiation. The edge of the top two graphene layers has increased disorder after the electron beam irradiation. The hole formed to the left of the interface, indicating that a layer in the ABC region was being sputtered but that this layer was not part of the 4-layered graphene structure to the right of the interface. This helps us to construct a picture of the relevant stacking sequences of the graphene layers in this region. Figure 4(ii, d) shows a second experimental image of the same area recorded with a different defocus value, and Figure 4(ii, e) and (ii, f) show image

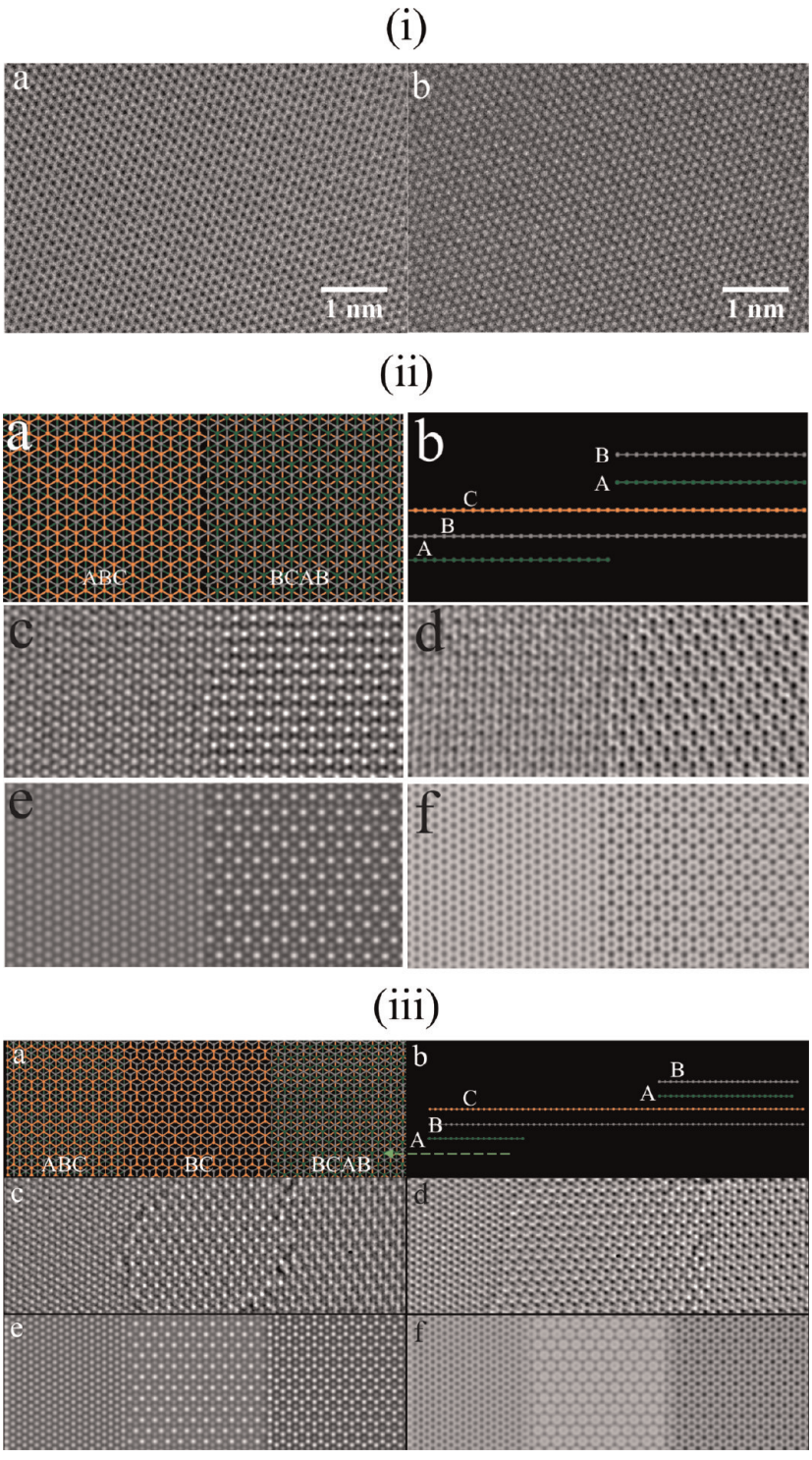

Figure 4. (i) (a, b) HRTEM images of ABC rhombohedral graphene taken at different defocus values, showing a contrast inversion. (ii) (a) Top and (b) side view of an atomic model of 3:4 ABC:BCAB few-layer graphene structure. (c) HRTEM image of a 3:4 ABC:BCAB few-layer graphene interface and (d) HRTEM image of the same area as in (c), but recorded at a different defocus. (e) Multislice image simulation of a 3:4 ABC:BCAB few-layer graphene structure calculated at 4 nm defocus corresponding to the HRTEM image in (c). (f) Multislice image simulation of a 3:4 ABC:BCAB few-layer graphene structure calculated at 1 nm defocus corresponding to the HRTEM image in (d). (iii) (a) Top and (b) side view of an atomic model of 3:2:4 ABC:BC:BCAB few-layer graphene structure. (c) HRTEM image of the interface region in (ii), following electron beam sputtering to open a hole in the middle region. (d) Same area as in (ii, c) but recorded at a different defocus. (e, f) Multislice image simulations based on the model in (ii, a) for (e) −3 nm defocus and (f) −1 nm defocus. Red hexagons with a green central spot are used in (ii, c)−(ii, f) to show matches between the experimental and simulated image contrast.

simulations based on the atomic model in (a), with defocus values of (e) −3 nm and (f) −1 nm. A red hexagon with a green central spot is overlaid on both experimental images and simulations to show correlated contrast features and

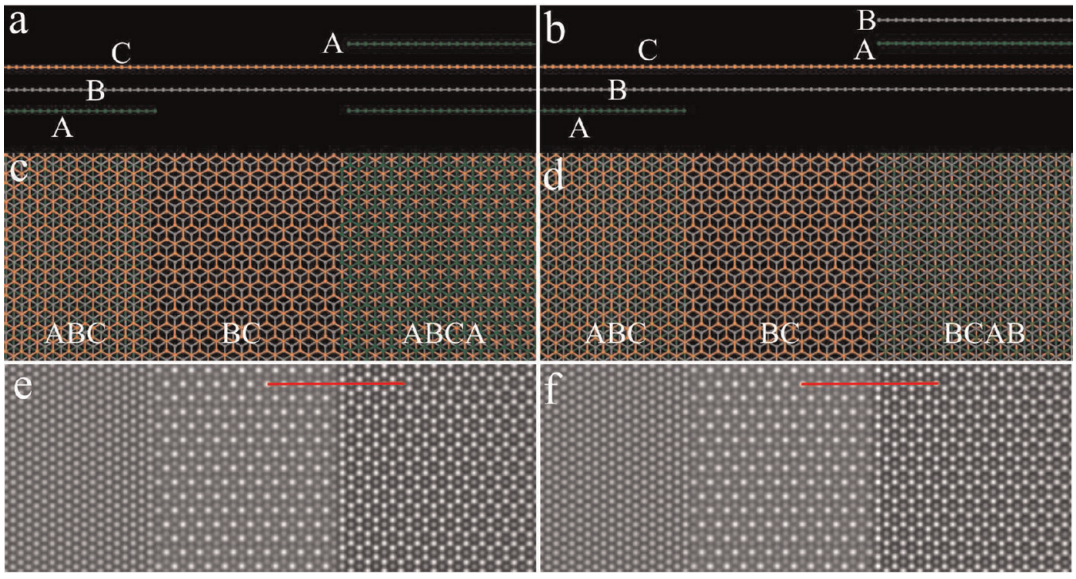

Figure 5. (a) Side view of an atomic model of an ABC:BC:ABCA graphene structure. (b) Side view of an atomic model of an ABC:BC:BCAB graphene structure. (c, d) Top views of the atomic models in (a) and (b) respectively. (e, f) Multislice image simulations based on the model in (c) and (d), respectively.

to highlight the excellent agreement between both images and their respective simulations.

Exposing the middle BC bilayer region by electron beam irradiation enables the determination of all atoms within the structure, as the contrast pattern of bilayer graphene can be directly related to its atomic structure by comparison of image simulations with the projected atomic model. This in turn enables us to determine the 3D structure of the material in this local region. Figure 5(a) and (b) show side views of atomic models with (a) ABC:BC:ABCA stacking sequences and (b) with an ABC:BC:BCAB stacking sequence. The difference between these is the 3D structure of the 4-layer region on the right. Figure 5(c) and (d) show top views of the atomic models in Figure 5(a) and (b), respectively. Figure 5(e) and (f) show the multislice image simulations of the atomic models in Figure 5(c) and (d), respectively. The red lines in Figure 5(e) and (f) mark the location where the rows of bright white spots in the BC bilayer region in the middle intersect the bright white hexagonal pattern in the 4-layer graphene structure on the right. For the BC:ABCA interface, Figure 5(e), this line intersects the middle of the hexagonal pattern in the ABCA region; however for the BC:BCAB interface, Figure 5(f), the line intersects part of the bright white spots in the hexagonal pattern. Our experimental image, Figure 4(iii, c), matches the simulation, Figure 5(c), and hence enables us to determine the exact 3D interface structure. The type of interface determined from these results agrees well with our previous studies in few-layer graphene samples grown by CVD, where we observed both direct bonding between graphene sheets and also overlapping of sheets on top of each other.[14]

CONCLUSION

In summary the results presented here reveal for the first time fully resolved atomic resolution images of both Bernal and rhombohedral stacking in few-layer graphene. We have shown that few-layer graphene grown by chemical vapor deposition contains ABC trilayer graphene, as well as 4-layer ABCA stacked graphene. The interface between the 3:4 layers of graphene contained only two directly bonded graphene sheets, with two unterminated sheets residing on the top and one unterminated sheet on the bottom. These studies also demonstrate that the use of a monochromator in low-voltage HRTEM leads to an increase in spatial resolution that is required to unambiguously assign layer stackings in complex multilayer graphene structures. This also suggests a way forward for accurate characterization of layer stackings in specifically fabricated few-layer graphene structures, which is a crucial step in developing tailored electronic properties.

METHODS

Graphene CVD. Copper foils (Alfa Aesar, product no. 42189, 99.999% purity) were loaded into a quartz tube located in a horizontal split-tube furnace. After purging the system with argon gas, 600 sccm of a hydrogen/argon gas mix (25% hydrogen) was introduced into the system. At a temperature of 1000 °C the quartz tube was shifted inward into the furnace, so that the sample resided in the hot zone, where it was annealed and reduced for 30 min to remove surface oxide. A methane/argon gas mixture (20% methane), with a flow rate of approximately 5–10 sccm, was then supplied, while continuing to maintain the 600 sccm hydrogen gas mix flow, for 3 min. The

sample was cooled to ambient temperature by shifting the quartz tube from the furnace and was left to rapidly cool under a hydrogen and argon atmosphere.

Graphene Transfer. Graphene was transferred from the copper foils by first drop-casting a solution of PMMA in toluene onto the graphene surface and allowing it to dry. The back of the copper foil was then rubbed with a cotton swab to remove the extra graphene layer. The copper was etched away in an hour by an iron(III) chloride solution (concentration of 0.1 g mL^{-1}). The graphene/PMMA film was then rinsed in deionized water and transferred to a concentrated hydrochloric acid solution (30%), in order to remove residual contaminants, such as iron from the etching solution. A further thorough rinsing in DI water was then performed. Transfer of the film to a holey silicon nitride TEM grid (Agar Scientific number Y5385) was done by attaching the grid to a lightly sticky pad (Gel-Pak gel-film WF-40-X8-A), which in turn was attached to a glass slide, and using this to "scoop" the film out of the DI water. The PMMA can then be removed by first applying acetone solvent and then by baking in air for 2−3 h at about 350 °C. The sample contained regions of mono-, bi-, tri-, and few-layer graphene.

Electron Microscopy. HRTEM imaging was performed using an Oxford-JEOL 2200MCO equipped with both probe and image spherical aberration correctors and a double-Wien filter monochromator, operated at an accelerating voltage of 80 kV. For all images reported with the monochromator on, a 5 μm slit was used to reduce the energy spread of the electron beam to 0.21 eV.

Conflict of Interest: The authors declare no competing financial interest.

Supporting Information Available: Details of microscope conditions are available free of charge *via* the Internet at http://pubs.acs.org.

Acknowledgment. J.H.W. thanks the Royal Society for support. Financial support from EPSRC (Grant EP/F028784/1) is gratefully acknowledged.

REFERENCES AND NOTES

1. Novoselov, K. S.; Geim, A. K.; Morozov, S. V.; Jiang, D.; Zhang, Y.; Dubonos, S. V.; Grigorieva, I. V.; Firsov, A. A. Electric Field Effect in Atomically Thin Carbon Films. *Science* **2004**, *22*, 666–669.
2. Oostinga, J. B.; Heersche, H. B.; Liu, X.; Morpurgo, A. F.; Vandersypen, L. M. K. Gate-Induced Insulating State in Bilayer Graphene Devices. *Nat. Mater.* **2008**, *7*, 151–157.
3. Craciun, M. F.; Russo, S.; Yamamoto, M.; Oostinga, J. B.; Morpurgo, A. F.; Tarucha, S. Trilayer Graphene is a Semimetal with a Gate-tunable Band Overlap. *Nat. Nanotechnol.* **2009**, *4*, 383–388.
4. Kumar, A.; Escoffier, W.; Poumirol, J. M.; Faugeras, C.; Arovas, D. P.; Fogler, M. M.; Guinea, F.; Roche, S.; Goiran, M.; Raquet, B. Integer Quantum Hall Effect in Trilayer Graphene. *Phys. Rev. Lett.* **2011**, *107*, 126806.
5. Bao, W.; Jing, L.; Velasco, J., Jr; Lee, Y.; Liu, G.; Tran, D.; Standley, B.; Aykol, M.; Cronin, S. B.; Smirnov, D.; *et al*. Stacking-Dependent Band Gap and Quantum Transport in Trilayer Graphene. *Nat. Phys.* **2011**, *7*, 948–952.
6. Jhang, S. H.; Craciun, M. F.; Schmidmeier, S.; Tokumitsu, S.; Russo, S.; Yamamoto, M.; Skourski, Y.; Wosnitza, J.; Tarucha, S.; Eroms, J.; *et al*. Stacking-Order Dependent Transport Properties of Trilayer Graphene. *Phys. Rev. B* **2011**, *84*, 161408(R).
7. Lui, C. H.; Li, Z.; Mak, K. F.; Cappelluti, E.; Heinz, T. F. Observation of an Electrically Tunable Band Gap in Trilayer Graphene. *Nat. Phys.* **2011**, *7*, 944–947.
8. Lui, C. H.; Li, Z.; Chen, Z.; Klimov, P. V.; Brus, L. E.; Heinz, T. F. Imaging Stacking Order in Few-Layer Graphene. *Nano Lett.* **2011**, *11*, 164–169.
9. Norimatsu, W.; Kusunoki, M. Selective Formation of ABC-Stacked Graphene Layers on SiC(0001). *Phys. Rev. B* **2010**, *81*, 161410(R).
10. Meyer, J. C.; Kisielowski, C.; Erni, R.; Rossell, M. D.; Crommie, M. F.; Zettl, A. Direct Imaging of Lattice Atoms and Topological Defects in Graphene Membranes. *Nano Lett.* **2008**, *8*, 3582–3586.
11. Liu, Z.; Suenaga, K.; Harris, P. J. F.; Iijima, S. Open and Closed Edges of Graphene Layers. *Phys. Rev. Lett.* **2009**, *102*, 015501.
12. Warner, J. H.; Rummeli, M. H.; Gemming, T.; Buchner, B.; Briggs, G. A. D. Direct Imaging of Rotational Stacking Faults in Few Layer Graphene. *Nano Lett.* **2009**, *9*, 102–106.
13. Krivanek, O. L.; Dellby, N.; Murfitt, M. F.; Chisholm, M. F.; Pennycook, T. J.; Suenaga, K.; Nicolosi, V. Gentle STEM: ADF Imaging and EELS at Low Primary Energies. *Ultramicroscopy* **2010**, *110*, 935–945.
14. Robertson, A. W.; Bachmatiuk, A.; Wu, Y. A.; Schaffel, F.; Rellinghaus, B.; Buchner, B.; Rummeli, M. H.; Warner, J. H. Atomic Structure of Interconnected Few Layer Graphene Domains. *ACS Nano* **2011**, *5*, 6610–6618.
15. Nelson, F.; Diebold, A. C.; Hull, R. Simulation Study of Aberration-Corrected High Resolution Transmission Electron Microscopy Imaging of Few-Layer Graphene Stacking. *Microsc. Microanal.* **2010**, *16*, 194–199.
16. Warner, J. H.; Rummeli, M. H.; Ge, L.; Gemming, T.; Montanari, B.; Harrison, N. M.; Buchner, B.; Briggs, G. A. D. Structural Transformations in Graphene Studied with High Spatial and Temporal Resolution. *Nat. Nanotechnol.* **2009**, *4*, 500–504.
17. Erni, R.; Rossell, M. D.; Nguyen, M.-T.; Blankenburg, S.; Passerone, D.; Hartel, P.; Alem, N.; Erickson, K.; Gannett, W.; Zettl, A. Stability and Dynamics of Small Molecules Trapped on Graphene. *Phys. Rev. B* **2010**, *82*, 165443.
18. Koskinen, P.; Malola, S.; Hakkinen, H. Evidence for Graphene Edges beyond Zigzag and Armchair. *Phys. Rev. B* **2009**, *80*, 073401.
19. Kim, K.; Lee, Z.; Regan, W.; Kisielowski, C.; Crommie, M. F.; Zettl, A. Grain Boundary Mapping in Polycrystalline Graphene. *ACS Nano* **2011**, *5*, 2142–2146.
20. Meyer, J. C.; Kurasch, S.; Park, H. J.; Skakalova, V.; Kunzel, D.; Grob, A.; Chuvilin, A.; Algara-Siller, G.; Roth, S.; Iwasaki, T.; *et al*. Experimental Analysis of Charge Redistribution Due to Chemical Bonding by High Resolution Transmission Electron Microscopy. *Nat. Mater.* **2011**, *10*, 209–215.
21. Girit, C. O.; Meyer, J. C.; Erni, R.; Rossell, M. D.; Kisielowski, C.; Yang, L.; Park, C.-H.; Crommie, M. F.; Cohen, M.; Louie, S. G.; *et al*. Graphene at the Edge: Stability and Dynamics. *Science* **2009**, *323*, 1705–1708.
22. Jinschek, J. R.; Yucelen, E.; Calderon, H. A.; Freitag, B. Quantitative Atomic 3-D Imaging of Single/Double Sheet Graphene Structure. *Carbon* **2011**, *49*, 556–562.
23. Warner, J. H. The Influence of the Number of Layers of Graphene on the Atomic Resolution Images Obtained from Aberration-Corrected High Resolution Transmission Electron Microscopy. *Nanotechnology* **2010**, *21*, 255707.